OPEN

ORIGINAL CONTRIBUTION

Artificial Intelligence Recognition System of Pelvic Autonomic Nerve During Total Mesorectal Excision

Fanghai Han, M.D., Ph.D.[1,2] • Guangyu Zhong, M.D.[1] • Shilin Zhi, M.M.[2] • Naiqian Han[3]
Yongjun Jiang, M.M.[3] • Jia'nan Tan, M.D.[1] • Lin Zhong, M.D.[2] • Shengning Zhou, M.D.[1]

1 Department of Gastrointestinal Surgery, The Affiliated Guangdong Second Provincial General Hospital of Jinan University, Guangzhou, Guangdong, China
2 Department of Gastrointestinal Surgery, Sun Yat-sen Memorial Hospital, Sun Yat-sen University, Guangzhou, China
3 Guangzhou Hans Medical Technology Co., Ltd., Guangzhou, China

BACKGROUND: The preservation of the pelvic autonomic nervous system in total mesorectal excision remains challenging to date. The application of laparoscopy has enabled visualization of fine anatomical structures; however, the rate of urogenital dysfunction remains high.

OBJECTIVE: To establish an artificial intelligence neurorecognition system to perform neurorecognition during total mesorectal excision.

DESIGN: This is a retrospective study.

SETTING: The study was conducted at a single hospital.

PATIENTS: Intraoperative images or video screenshots of patients with rectal cancer admitted to the Department of Gastrointestinal Surgery, Sun Yat-sen Memorial Hospital, Sun Yat-sen University, between January 2016 and December 2023, were retrospectively collected.

MAIN OUTCOME MEASURE: Mean intersection over union, precision, recall, and F1 of the model.

RESULTS: A total of 1424 high-quality intraoperative images were included in the training group. The proposed model was obtained after 700 iterations. The mean intersection over union was 0.75, and it slowly increased with an increase in training time. The precision and recall of the nerve category were 0.7494 and 0.6587, respectively, and the F1 was 0.7011. The video prediction shows that the model achieves a high accuracy rate, which could facilitate effective neurorecognition.

LIMITATION: This was a single-center study.

CONCLUSIONS: The artificial intelligence model for real-time visual neurorecognition in total mesorectal excision was successfully established for the first time in China. Better identification of these autonomic nerves should allow for better preservation of urogenital function, but further research is needed to validate this claim. See **Video Abstract**.

Supplemental digital content is available for this article. Direct URL citations appear in the printed text, and links to the digital files are provided in the HTML and PDF versions of this article on the journal's website (www.dcrjournal.com).

Funding/Support: None reported.

Financial Disclosure: None reported.

Fanghai Han and Guangyu Zhong contributed equally.

Correspondence: Fanghai Han, M.D., Ph.D., Department of Gastrointestinal Surgery, The Affiliated Guangdong Second Provincial General Hospital of Jinan University, Guangzhou, Guangdong 510317, China; Sun Yat-sen Memorial Hospital, Sun Yat-sen University, No.107 Yanjiang West Rd, Guangzhou 510000, China. E-mail: fh_han@163.com

Dis Colon Rectum 2025; 68: 308–315
DOI: 10.1097/DCR.0000000000003547

SISTEMA DE RECONOCIMIENTO CON INTELIGENCIA ARTIFICIAL DEL NERVIO AUTÓNOMO PÉLVICO DURANTE LA ESCISIÓN TOTAL DEL MESORRECTAL

ANTECEDENTES: La preservación del sistema nervioso autónomo pélvico en la escisión mesorrectal total sigue siendo un desafío hasta la fecha. La aplicación de la laparoscopia ha permitido la visualización de estructuras anatómicas finas; sin embargo, la tasa de disfunción urogenital sigue siendo alta.

OBJETIVO: Establecer un sistema de reconocimiento neurológico con inteligencia artificial para realizar el reconocimiento neurológico durante la escisión mesorrectal total.

DISEÑO Y ESCENARIO: Este estudio retrospectivo se realizó en un solo hospital.

PACIENTES: Se recopilaron retrospectivamente imágenes intraoperatorias o capturas de pantalla de video de pacientes con cáncer de recto ingresados en el Departamento de Cirugía Gastrointestinal, del Hospital Memorial Sun Yat-sen, de la Universidad Sun Yat-sen, entre enero de 2016 y diciembre de 2023.

PRINCIPALES MEDIDAS DE VALORACIÓN: Intersección media sobre unión, precisión, recuperación y F1 del modelo.

RESULTADOS: Se incluyeron un total de 1424 imágenes intraoperatorias de alta calidad en el grupo de entrenamiento. El modelo propuesto se obtuvo después de 700 interaciones. La intersección media sobre la unión fue de 0,75 y aumentó lentamente con el aumento del tiempo de entrenamiento. La precisión y la recuperación de la categoría de nervio fueron de 0,7494 y 0,6587, respectivamente, y el F1 fue de 0,7011. A partir de la predicción del video, podemos observar que el modelo logra una alta tasa de precisión, lo que podría facilitar el neurorreconocimiento efectivo.

LIMITACIÓN: Este fue un estudio de un solo centro.

CONCLUSIÓN: El modelo de inteligencia artificial para el neurorreconocimiento visual en tiempo real en la escisión mesorrectal total se estableció con éxito por primera vez en China. Una mejor identificación de estos nervios autónomos debería permitir una mejor preservación de la función urogenital, pero se necesita más investigación para validar esta afirmación. *(Traducción--Ingrid Melo)*

KEY WORDS: Artificial intelligence; Neurorecognition; Pelvic autonomic nervous system; Rectal cancer; Total mesorectal excision.

Colorectal cancer, the third most common diagnosed cancer globally and the second most common cancer in China, accounts for approximately one-third to half of all rectal cancers (RCs).[1–3] Currently, total mesorectal excision (TME) and perioperative chemoradiotherapy are the primary treatments for RCs.[4,5] Because standardized and effective treatments have resulted in a 5-year survival rate of approximately 70% for all stages of RC,[6] postoperative urogenital dysfunction due to nerve injury during TME needs immediate attention.[7]

The adequate preservation of the pelvic autonomic nerve (PAN) during TME remains challenging for GI surgeons; however, it mainly depends on the experience and expertise of the surgeons.[8,9] The application of laparoscopy has enabled visualization of fine anatomical structures, such as the PAN, owing to their high resolution, magnification, and stereoscopic imaging. However, urinary and sexual dysfunction rates after laparoscopic TME are 10% to 30% and 20% to 50%, respectively.[10,11] Advancements in surgical equipment have not effectively assisted in the preservation of PAN. Inadequate visualization of the surgical field owing to a physiologically narrow pelvis and intraoperative bleeding may increase the risk of nerve injury. The nerve is usually nonregenerative; therefore, the urogenital dysfunction resulting from nerve injury is often difficult to treat and greatly reduces the quality of life (QOL) of patients with RC.

In recent years, artificial intelligence (AI) has been widely used in the medical field, mainly through machine learning and image recognition.[12–14] This technology has been used most frequently in lesser complex procedures, such as the use of GoNoGoNet for safe cholecystectomy.[15] Kolbinger et al[16] confirmed the feasibility of AI in robotic-assisted rectal resection. However, due to low visibility and unclear differences from surrounding tissues, the recognition of PAN in RC through computer vision is still being explored. Kojima et al[17] established recognition models of the hypogastric nerve and superior hypogastric plexus through AI but did not target the pelvic plexus, pelvic splanchnic nerve (PSN), and neurovascular bundle (NVB). The recognition of the pelvic plexus is equally important for the preservation of urinary and sexual function of patients with RC. AI can aid in the preservation of nerve structures through rapid and more secure identification of autonomic nerves. Literature on whole PAN identification during TME is currently lacking.[18] Therefore, we aimed to establish an AI neurorecognition system (AINS) to identify whole PAN and perform neurorecognition during TME by delineating intraoperative autonomic nerve images and machine learning.

MATERIALS AND METHODS

Study Design and Patients

This study was approved by the Ethics Committee of the Sun Yat-sen Memorial Hospital, Sun Yat-sen University. Data from patients with RC admitted to the Department of Gastrointestinal Surgery, Sun Yat-sen Memorial Hospital, Sun Yat-sen University, between January 2016 and December 2023 were retrospectively collected. Patients who met the following criteria were included in the study: 1) aged 18 years or older, 2) presence of histopathologically confirmed RC, 3) history of 3-dimensional (3D) laparoscopic TME surgery, and 4) availability of clear surgical screenshots or surgical videos.

Development of the AINS Algorithm

This algorithm includes 3 processing steps: data annotation, data preprocessing, and model training and verification.

Data annotation. Intraoperative images or video screenshots of different patients recorded at 1920 × 1080p resolution, which clearly shows the PAN, were collected. After

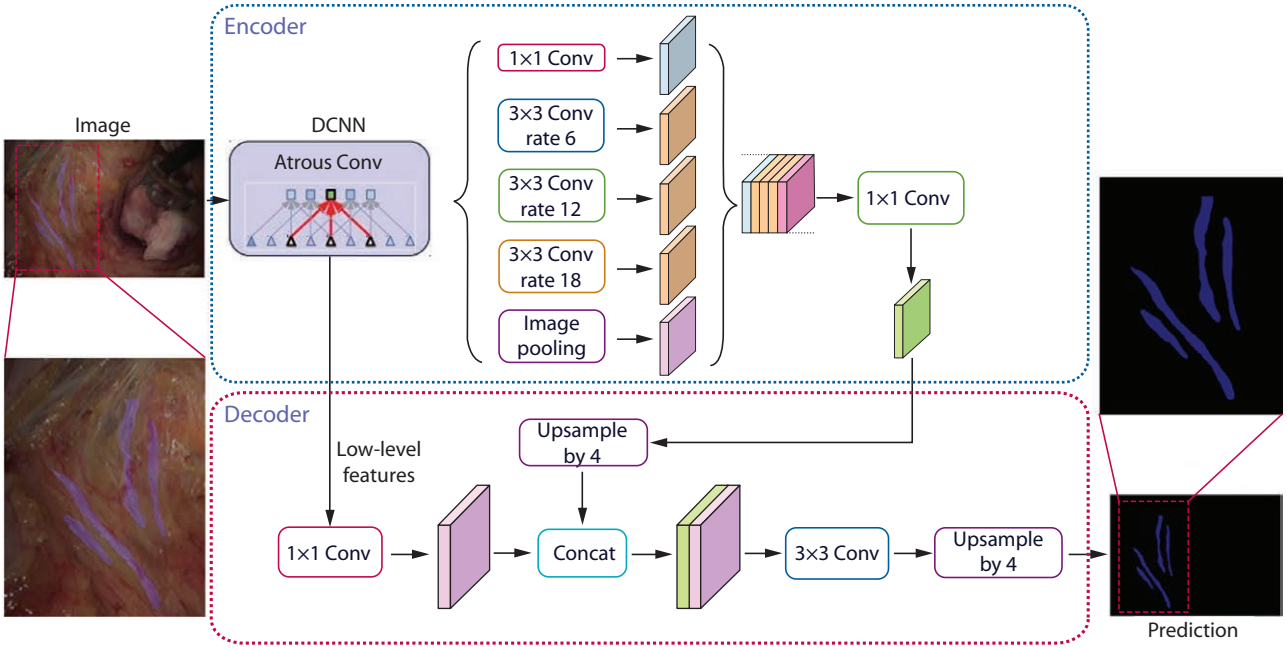

FIGURE 1. Schematic diagram of image sketching, model training, and model recognition. Conv = convolution, which is a mathematical operation used extensively in convolutional neural networks (CNNs). Concat = concatenation, which refers to combining feature maps from different layers or branches of a convolutional neural network (CNN) along the channel dimension. DCNN = deep convolutional neural networks, which is a type of deep learning model extensively used in computer vision tasks like image classification, object detection, and semantic segmentation

the exclusion of low-quality images, such as those with poor resolution, blurring, and bleeding, 1780 high-quality images were included. The images were randomly divided into training and validation groups in a ratio of 4:1 (1424 images in the training group and 356 in the verification group). The PAN images in the training groups were delineated by a team of 2 experienced GI professors (with >10 years of experience). Annotations from professors contributed to the subsequent model construction. Disagreements between them were resolved by a third GI professor with 20 years of experience to determine the final neural delineation.

Data preprocessing. The similarity coefficients among images were computed using the OpenCV project, and the cutoff for deduplication was defined at 0.58. Images with a similarity coefficient greater than the cutoff value were removed from the model. The images were rotated at different clockwise rotation angles to introduce extra nerve variables and increase the robustness of the model to face different orientations. Mirroring included horizontal, vertical, and central mirror images. This procedure can enrich the diversity of the data set and expose the model to different viewpoints of nerves, thereby increasing its generalizability.

Model Training and Verification

Model selection. DeepLabv3+, a series of semantic segmentation algorithms proposed by the Google team that uses a grouped convolutional network to speed up recognition, was selected as the model architecture for this study.[19,20] The core network adopted RestNet50_Vd (residual network), which is characterized by ease of optimization and the ability to increase accuracy by adding considerable depth (Fig. 1).

Pretrained model. The Pascal VOC project was used for the pretrained model.[21] The Pascal VOC data set includes 30,000 images of eye identifiers and 80,000 objects in 20 categories. Pretraining the model facilitates its learning of business characteristics.

Model verification. Parameters such as the mean intersection over union (mIOU), precision, recall rate, and F1 index were calculated for model evaluation.

mIOU: An evaluation index of semantic segmentation that represents the average intersection ratio. The ratio of the intersection and union of the set of true values and predicted values. This value ranges between 0 and 1; the higher the value, the better the model.

Precision: This indicates the proportion of the true positive samples among the predicted positive samples.

Recall rate: Refers to the proportion of positive cases in the sample that were correctly predicted, which is similar to sensitivity.

F1 index: The F1 score was calculated as the harmonic mean of precision and recall, which is calculated using the following formula: 2 × precision × recall/(precision þ recall).

TABLE 1. Scores of the 2 groups as evaluated by the GI professor

Score	*A*	*B*	*p*
1	67 (18.82%)	43 (12.07%)	0.000
2	143 (40.17%)	106 (29.78%)	
3	93 (26.12%)	131 (36.80%)	
4	53 (14.89%)	76 (21.35%)	

Group A consists of younger GI surgeons (<10 y) and group B represents model. Categorical variables in both groups were compared using the χ^2 tests. $P < 0.05$ was considered statistically significant.

To clarify the differences in recognition time and accuracy, the PAN region in the validation group images was delineated by a team of 2 younger GI surgeons (with <10 years of experience). The GI surgery professors used Likert scores to evaluate the recognition of model identification and delineation by young doctors (1: not delineated, 2: identified a small part of the nerve, 3: identified most of the nerves, and 4: identified all nerves; Table 1). The younger surgeons' annotations acted as an evaluation compared to those of the AINS.

A pathological examination was performed to confirm the accuracy of the neural output of the AINS. Nerve branches to the rectum from the pelvic plexus and the hypogastric nerve that were successfully identified by the model and within the standard TME resection range were marked during surgery using a small Hem-o-lok. After surgery, pathological examinations of the labeled tissues from the specimens were performed.

Statistical Analysis

The mIOU, precision, recall rate, and F1 index were calculated to evaluate the AINS model.[16,18] The model parameters were compared with those of young GI surgeons (<10 years of experience). χ^2 tests were used to compare the categorical variables between the 2 groups. The kappa concordance test was used to analyze the consistency of neural annotation by 2 experienced GI professors. All statistical tests were performed using the R software (version 3.6.1). A p value of <0.05 indicated statistical significance.

RESULTS

A total of 1780 images were included and divided into training and validation groups in a ratio of 4:1; 1424 high-quality images were included in the training group (the characteristic of patients from whom the images were obtained was supplemented in Table 2). The kappa value of consistency evaluation of GI professors on neural annotation was 0.78, indicating that interobserver agreement was strong. After 700 iterations, the current model was obtained, and the parameters are summarized in Supplemental Figure 1 at http://links.lww.com/DCR/C439.

TABLE 2. Patient demographics and clinical characteristics

Characteristic	*N = 244*
Age, y	57.42 ± 8.52
Sex	
Male	168 (68.9%)
Female	76 (31.1%)
BMI	23.00 ± 2.71
ASA score	
I	154 (63.1%)
II	74 (30.3%)
III	16 (6.6%)
Tumor distance from AV	
Low ≤8 cm	165 (67.6%)
Middle 8–12 cm	79 (32.4%)
Surgical procedure	
Low anterior resection	237 (97.1%)
abdominoperineal resection	4 (1.6%)
Intersphincteric resection	3 (1.2%)
Clinical stage	
I	56 (23.0%)
II	73 (29.9%)
III	115 (47.1%)
cT	
1	4 (1.6%)
2	71 (29.1%)
3	169 (69.3%)
cN	
0	125 (51.2%)
1	79 (32.4%)
2	40 (16.4%)
Adjuvant chemoradiotherapy	133 (54.5%)

Data presented as absolute number of patients (%) or mean ± SD. ASA score is calculated using the ASA physical status classification system.
AV = anal verge; cN = clinical N stage; cT = clinical T stage.

As shown in Figure 1, the mIOU of this training was 0.75, which gradually increased with an increase in training time. The precision of the background category was 0.9754, which is relatively ideal, whereas the precision of the nerve category was 0.7494. The recall rate of the background category was 0.9840 and that of the nerve category was 0.6587. Accordingly, the F1 index of our model was 0.7011. The recognition results outlined by the professor in comparison to our model are shown in Figure 2, Supplemental Figure 2 at http://links.lww.com/DCR/C440, and Supplemental Figure 3 at http://links.lww.com/DCR/C441.

Pathological Examination

Pathological examinations of the labeled tissues were performed to confirm that the tissue recognized by the model was a nerve (see Supplemental Fig. 4 at http://links.lww.com/DCR/C442). We only made corresponding judgments during surgery when suspected nerve invasion or rare autonomic nerve branches to the rectum were detected. In this study, a total of 17 patients were identified, including 14 cases of autonomic nervous system, 2 cases of small blood vessels, and 1 case of membrane fiber, with a correct proportion of 82.35%.

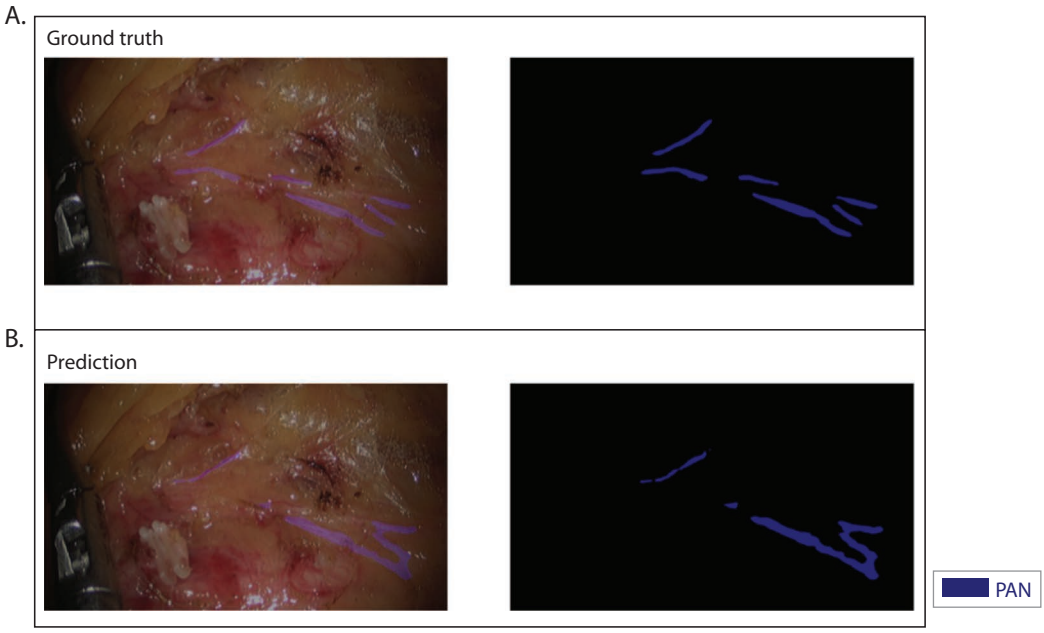

FIGURE 2. Recognition of nerves at the root of the inferior mesenteric artery. A, The recognition results annotated by the professor of GI surgery (ground truth: truth of nerve course). B, The recognition results of our model (prediction of nerve course by model). PAN = pelvic autonomic nerve.

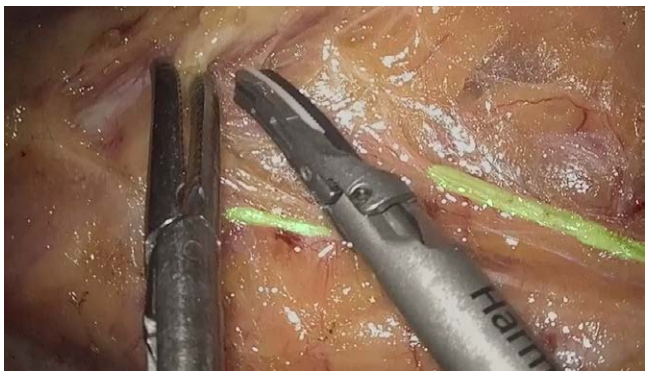

FIGURE 3. Screenshot of the prediction video. Autonomic nerves at the root of the inferior mesenteric artery are shown as green areas.

FIGURE 4. Screenshot of the prediction video. The right hypogastric nerve is shown as a green area.

Validation Model vs Younger GI Surgeons (Experience <10 y)

The overall accuracy, precision, recall, and F1 score of the model were 0.9609, 0.7494, 0.6587, and 0.7011, respectively. The precision, recall, and F1 score of the young GI surgeons' group were 0.6548, 0.3508, and 0.4568, respectively. The validation set had 356 images, and the time for model recognition was 3 minutes, whereas young surgeons needed 25 minutes to identify the images in the validation set.

Validation of the Model in Surgical Videos

The primary objective of our study was to establish a neuromonitoring and real-time recognition system for the TME (Videos 1–4 at http://links.lww.com/DCR/C473, http://links.lww.com/DCR/C474, http://links.lww.com/DCR/C475, http://links.lww.com/DCR/C476 and http://links.lww.com/DCR/C477). We can observe from the application of the AINS to our video that the model achieves a high accuracy rate, which is crucial for monitoring and recognition (Figs. 3 and 4). Moreover, recognition of the sympathetic plexus around the roots of the inferior mesenteric artery, superior hypogastric plexus, bilateral hypogastric nerves, pelvic plexus, NVB, and PSN was remarkable. The practice of dual-screen display in the operating room was uploaded (see Video 5). One screen is the conventional display and the other screen is the display of the navigation system (green area). The real-time intraoperative videos are displayed for neural recognition so that surgeons can avoid nerve damage.

DISCUSSION

This novel attempt was successful for TME and autonomic nerve preservation (ANP) in RCs. Combining the key and

difficult issues of preserving the PAN in TME+ANP with the current application of AI, a novel AINS was successfully developed through the fine delineation of the PAN in our high-definition surgical images and model training. The model was applied to video verification, which could identify the PAN in the surgical video. Furthermore, the AINS was connected to the laparoscope for a dual-screen display to enable routine intraoperative observation and for predicting the nerve route of the model, which plays an important role in neurorecognition in TME+ANP (Video 5).

The preservation of PAN in the TME+ANP for RC remains unsolved. Urogenital and anal continence dysfunction due to intraoperative PAN injuries is an important factor leading to a decline in postoperative QOL. The corresponding PAN in TME+ANP mainly includes the sympathetic plexus at the root of the inferior mesenteric artery, superior hypogastric plexus, hypogastric nerve, pelvic plexus, PSN, and NVB. Aurore et al[22] suggested that the PAN has many variations; approximately 25% of people have accessory hypogastric nerves, and approximately 18% of PSNs originate from S1. Röthlisberger et al[23] suggested that the pelvic plexus sends out the NVB in several ways that are morphologically different. Corresponding guidelines or consensuses on how to preserve the PAN are currently lacking. Based on our empirical anatomical observations, the autonomic nerves sent out branches to anastomose with each other, presenting a "network." Therefore, we proposed that "TME + network ANP" preserve not only the trunk of the autonomic nerve but also its branches and blood supply.[24] Notably, ANP performed solely based on clinical experience or previous histological knowledge often yielded unsatisfactory results. Several studies have explored how to better preserve the PAN during TME+ANP.[25,26] Some studies have focused on individualized preoperative magnetic resonance neuroimaging to clarify the course and variation of PAN.[27,28] However, nerve variations and small branches are difficult to visualize. Other studies focused on intraoperative advances and explored the impact of advancements in surgical equipment for TME+ANP.[29] Compared with open surgery, the application of 3D laparoscopy can reduce the rate of postoperative urogenital dysfunction; however, the incidence rate remains high, and the rates of urinary and sexual dysfunction are 10% to 36% and 10% to 30%,[10] respectively. Approximately one-third of these injuries were due to surgery, and urogenital dysfunction rates varied widely in different studies. Despite stereoscopic vision and high resolution, the surgery is complicated and cannot be performed exactly as planned in obese patients with a narrow, deep pelvis, further complicated by intraoperative bleeding or inadequate exposure. A European study on the visibility rate of the PAN during TME indicated that the visibility rate of many parts was low, such as the NVB (31.8%) and PSNs (12.9%), which are mainly preserved on the basis of personal experience when they are not visible.[30] Attempts have been made previously to establish intraoperative nerve monitoring to avoid injury; however, it has not been extensively used because of the complexity of the operation, tissue damage, and the inability to monitor delicate pelvic nerves.[31] Therefore, we aimed to build an AINS model to recognize PAN without physical or chemical damage to the nerves.

AI can learn various unique features of a certain disease or structure by training AI models through manual annotations by medical experts.[32,33] Kojima et al[17] established recognition models of the hypogastric nerve and superior hypogastric plexus through AI but did not target the pelvic plexus, PSN, or NVB. Therefore, we explored whether AI could be used for intraoperative neuromonitoring and recognition for whole PAN in TME+ANP. This was the first study in China that attempted PAN monitoring and neurorecognition using AI for TME+ANP. We primarily performed PAN delineation training on high-definition surgical images recorded using 3D laparoscopy. The anatomical structure of the PAN is complex and diverse; the thickness, branches, and blood supply of the nerves differ in different parts. Therefore, identifying PAN through the lens during surgery warrants a long learning curve, and not all GI surgeons can judge it in time, especially those who do not perform many surgeries or lack high-definition laparoscopy. The PAN mainly comprised white fibers running on the fascia (shown as light white fibers) under laparoscopy, and some were accompanied by a vascular supply (shown as red fibers attached to white fibers). Owing to the large heterogeneity of the nerve and its light color, distinguishing it from the surrounding fascia, tissues, and organs is difficult. Assessing autonomic nerves is time-consuming, even for experienced GI surgeons, and errors are inevitable. This requires a wealth of clinical experience and adequate anatomical knowledge of the PAN rather than seniority. Therefore, the heterogeneity of the nerve and the indistinct distinction between the autonomic nerve and the surrounding tissues pose a great challenge to nerve delineation.

The PAN was delineated by 2 experienced GI surgeons. DeepLabv3+, a classic graph segmentation model used in the industry that consists of a series of semantic segmentation algorithms proposed by the Google team, was selected for our study. Our results indicated that the overall recognition accuracy, precision, and recall of the trained model were 0.9609, 0.7494, and 0.6587, respectively, and the calculated F1 index was 0.7011.

Although the values of the parameters in this model were not high, the neural recognition was complex. The nerve course may not be completely visualized in some images owing to factors such as being out of focus, reflection issues, and angle changes. Nevertheless, the evaluation of the professors of GI surgery revealed that this model demonstrated good results in surgical videos and was able to recognize almost all autonomic nerves. This

could be attributed to a few reasons. First, a video is a continuous image, not just an image, and a 1-second video may contain 5 to 10 images. Our model identified all images, and its quantitative advantage compensated for the lack of accuracy. For instance, when there are 5 images in one second, our model should have a precision of $1 - (1 - 0.7494)^5$ at this site with a result of 0.999, and the same recall should be $1 - (1 - 0.6587)^5$ with a result of 0.995. Therefore, the model plays a considerable role in neural recognition. Second, images and videos during the operation were captured by the camera-holding surgeon by constantly adjusting the focus and angle. Although the nerves in different parts may not be displayed well simultaneously, the surgical team can make certain adjustments to enhance the display. Third, this procedure requires sufficient traction and exposure. The surgeon and assistant will have sufficient coordination and adjustment during surgical separation so that the autonomic nerves will be fully displayed and monitored. Therefore, our model can identify the PAN during TME+ANP surgery and assist in intraoperative neurorecognition. Large variations exist in the pelvic plexus, and it is sometimes difficult to determine the anatomical range of the pelvic plexus. Preventing intraoperative damage to the PAN is imperative, as recovering postoperative urogenital function is difficult after a nerve injury. The application of this system is expected to promote network ANP and improve the near- and long-term QOL. In the past, many young surgeons did not receive sufficient guidance because of a lack of learning methods. If this system can be promoted, it will deepen our understanding of the PAN and is expected to promote the standardized preservation of autonomic nerves in TME+ANP surgery for RCs. Moreover, we plan to conduct a multicenter randomized controlled trial to determine whether the application of this model in TME surgery can better preserve the autonomic nerves and reduce the rate of postoperative urogenital dysfunction.

The main limitation of this study was that the number of images was insufficient. Another limitation is the lack of external validation. Currently, comprehensive recognition systems for the TME are lacking. Further developments will be made for the precise recognition of fascia separation layers, lymph node recognition, and integration with our current recognition system for TME+ANP comprehensive recognition.

CONCLUSIONS

This study was the first in China to successfully establish a new real-time AINS during TME+ANP. Better identification of these autonomic nerves should allow for better preservation of urogenital function, but further research is needed to validate this claim.

REFERENCES

1. Sung H, Ferlay J, Siegel RL, et al. Global cancer statistics 2020: GLOBOCAN estimates of incidence and mortality worldwide for 36 cancers in 185 countries. *CA Cancer J Clin*. 2021;71:209–249.
2. Chen W, Zheng R, Baade PD, et al. Cancer statistics in China, 2015. *CA Cancer J Clin*. 2016;66:115–132.
3. Qiu H, Cao S, Xu R. Cancer incidence, mortality, and burden in China: a time-trend analysis and comparison with the United States and United Kingdom based on the global epidemiological data released in 2020. *Cancer Commun (Lond)*. 2021;41:1037–1048.
4. Heald RJ, Husband EM, Ryall RD. The mesorectum in rectal cancer surgery--the clue to pelvic recurrence? *Br J Surg*. 1982;69:613–616.
5. Heald RJ, Ryall RD. Recurrence and survival after total mesorectal excision for rectal cancer. *Lancet*. 1986;1:1479–1482.
6. Siegel RL, Miller KD, Jemal A. Cancer statistics, 2020. *CA Cancer J Clin*. 2020;70:7–30.
7. Wiltink LM, Nout RA, van der Voort van Zyp JRN, et al. Long-term health-related quality of life in patients with rectal cancer after preoperative short-course and long-course (chemo) radiotherapy. *Clin Colorectal Cancer*. 2016;15:e93–e99.
8. Chew M-H, Yeh Y-T, Lim E, Seow-Choen F. Pelvic autonomic nerve preservation in radical rectal cancer surgery: changes in the past 3 decades. *Gastroenterol Rep (Oxf)*. 2016;4:173–185.
9. Lee DK, Jo MK, Song K, Park JW, Moon S-M. Voiding and sexual function after autonomic-nerve-preserving surgery for rectal cancer in disease-free male patients. *Korean J Urol*. 2010;51:858–862.
10. Luca F, Craigg DK, Senthil M, et al. Sexual and urinary outcomes in robotic rectal surgery: review of the literature and technical considerations. *Updates Surg*. 2018;70:415–421.
11. Galata C, Vassilev G, Haas F, et al. Clinical, oncological, and functional outcomes of Da Vinci (Xi)-assisted versus conventional laparoscopic resection for rectal cancer: a prospective, controlled cohort study of 51 consecutive cases. *Int J Colorectal Dis*. 2019;34:1907–1914.
12. Iacucci M, Parigi T, Del Amor R, et al. Artificial intelligence enabled histological prediction of remission or activity and clinical outcomes in ulcerative colitis. *Gastroenterology*. 2023;164:1180–1188.e2.
13. Vachon C, Scott C, Norman A, et al. Impact of artificial intelligence system and volumetric density on risk prediction of interval, screen-detected, and advanced breast cancer. *J Clin Oncol*. 2023;41:3172–3183.
14. Adams S, Stone E, Baldwin D, Vliegenthart R, Lee P, Fintelmann F. Lung cancer screening. *Lancet*. 2023;401:390–408.
15. Laplante S, Namazi B, Kiani P, et al. Validation of an artificial intelligence platform for the guidance of safe laparoscopic cholecystectomy. *Surg Endosc*. 2023;37:2260–2268.
16. Kolbinger FR, Bodenstedt S, Carstens M, et al. Artificial intelligence for context-aware surgical guidance in complex robot-assisted oncological procedures: an exploratory feasibility study. *Eur J Surg Oncol*. 2024;50:106996.
17. Kojima S, Kitaguchi D, Igaki T, et al. Deep-learning-based semantic segmentation of autonomic nerves from laparoscopic images of colorectal surgery: an experimental pilot study. *Int J Surg*. 2023;109:813–820.

18. Quero G, Mascagni P, Kolbinger FR, et al. Artificial intelligence in colorectal cancer surgery: present and future perspectives. *Cancers (Basel)*. 2022;14:3803.
19. Wang J, Liu X. Medical image recognition and segmentation of pathological slices of gastric cancer based on Deeplab v3+ neural network. *Comput Methods Programs Biomed*. 2021;207: 106210.
20. Czajkowska J, Badura P, Korzekwa S, Płatkowska-Szczerek A. Automated segmentation of epidermis in high-frequency ultrasound of pathological skin using a cascade of DeepLab v3+ networks and fuzzy connectedness. *Comput Med Imaging Graph*. 2022;95:102023.
21. Chen C, Yang X, Zhang J, Dong B, Xu C. Category knowledge-guided parameter calibration for few-shot object detection. *IEEE Trans Image Process*. 2023;32:1092–1107.
22. Aurore V, Röthlisberger R, Boemke N, et al. Anatomy of the female pelvic nerves: a macroscopic study of the hypogastric plexus and their relations and variations. *J Anat*. 2020;237:487–494.
23. Röthlisberger R, Aurore V, Boemke S, et al. The anatomy of the male inferior hypogastric plexus: what should we know for nerve sparing surgery. *Clin Anat*. 2018;31:788–796.
24. Han F, Zhou S, Zhong G, et al. Three-dimensional versus two-dimensional laparoscopic surgery for rectal cancer: better promote postoperative sexual and urinary function of a propensity-matched study. *Am J Cancer Res*. 2022;12:3148–3163.
25. Fleming C, Cullinane C, Lynch N, Killeen S, Coffey J, Peirce C. Urogenital function following robotic and laparoscopic rectal cancer surgery: meta-analysis. *Br J Surg*. 2021;108:128–137.
26. Morelli L, Ceccarelli C, Di Franco G, et al. Sexual and urinary functions after robot-assisted versus pure laparoscopic total mesorectal excision for rectal cancer. *Int J Colorectal Dis*. 2016;31:913–915.
27. Bertrand M, Macri F, Mazars R, Droupy S, Beregi J, Prudhomme M. MRI-based 3D pelvic autonomous innervation: a first step towards image-guided pelvic surgery. *Eur Radiol*. 2014;24: 1989–1997.
28. Yamashita R, Isoda H, Arizono S, et al. Selective visualization of pelvic splanchnic nerve and pelvic plexus using readout-segmented echo-planar diffusion-weighted magnetic resonance neurography: a preliminary study in healthy male volunteers. *Eur J Radiol*. 2016;86:52–57.
29. Wijsmuller A, Giraudeau C, Leroy J, et al. A step towards stereotactic navigation during pelvic surgery: 3D nerve topography. *Surg Endosc*. 2018;32:3582–3591.
30. Cheung YM, Lange MM, Buunen M, Lange JF. Current technique of laparoscopic total mesorectal excision (TME): an international questionnaire among 368 surgeons. *Surg Endosc*. 2009;23:2796–2801.
31. Kneist W, Ghadimi M, Runkel N, et al; NEUROS Study Group. Pelvic intraoperative neuromonitoring prevents dysfunction in patients with rectal cancer: results from a multicenter, randomized, controlled clinical trial of a NEUROmonitoring System (NEUROS). *Ann Surg*. 2023;277:e737–e744.
32. Roth H, Xu Z, Tor-Díez C, et al. Rapid artificial intelligence solutions in a pandemic—the COVID-19-20 lung CT lesion segmentation challenge. *Med Image Anal*. 2022;82: 102605.
33. Yang Y, Yuan Y, Zhang G, et al. Artificial intelligence-enabled detection and assessment of Parkinson's disease using nocturnal breathing signals. *Nat Med*. 2022;28:2207–2215.